Three distinct sarcomeric patterns of skeletal muscle revealed by SHG and TPEF microscopy.

Gaëlle Recher, Denis Rouède, Patrick Richard, Antoine Simon, Jean-Jacques Bellanger, François Tiaho

Three distinct sarcomeric patterns of skeletal muscle revealed by SHG and TPEF Microscopy

Gaëlle Recher[1], Denis Rouède[2], Patrick Richard[2], Antoine Simon[3], Jean-Jaques Bellanger[3], François Tiaho[1]

[1]*Equipe SCANING, UMR UR1-CNRS 6026*
[2]*Institut de Physique de Rennes, UMR UR1-CNRS 6251*
[3]*Laboratoire Traitement du Signal et de l'Image, UMR UR1-INSERM U642*
Université de Rennes1, Campus de Beaulieu, 35042 Rennes Cedex, France
francois.tiaho@univ-rennes1.fr

Abstract: We have extensively characterized the sarcomeric SHG signal as a function of animal species (rat versus xenopus), age (adult versus larval) and tissue preparation (fixed or fresh) and we found that the main feature of this signal is a single peak per mature sarcomere (about 85% of all sarcomeres). The remaining (15%) was found to be either double peak per mature sarcomere or mini sarcomeres (half of a sarcomere) using α-actinin immuno detection of the Z-band. The mini sarcomeres are often found in region of pitchfork-like SHG pattern. We suggest that double peak SHG pattern could indicate regions of sarcomeric proteolysis whereas pitchfork-like SHG pattern could reveal sarcomeric assembly.

OCIS codes: (180.0180) Microscopy; (190.4160) Multiharmonic generation; (170.0170) Medical optics and biotechnology

References and links

1. P. J. Campagnola, A. C. Millard, M. Terasaki, P. E. Hoppe, C. J. Malone, and W. A. Mohler, "Three-dimensional high-resolution second-harmonic generation imaging of endogenous structural proteins in biological tissues," Biophys. J **82**, 493-508 (2002).
2. P. J. Campagnola and L. M. Loew, "Second-harmonic imaging microscopy for visualizing biomolecular arrays in cells, tissues and organisms," Nature biotechnology **21**, 1356-1360 (2003).
3. W. Mohler, A. C. Millard, and P. J. Campagnola, "Second harmonic generation imaging of endogenous structural proteins," Methods **29**, 97-109 (2003).
4. F. Tiaho, G. Recher, and D. Rouède, "Estimation of helical angles of myosin and collagen by second harmonic generation imaging microscopy," Opt. Express **15**, 12286-12295 (2007), http://www.opticsinfobase.org/oe/abstract.cfm?URI=oe-15-19-12286.
5. G. Cox, N. Moreno, J. Feijó, "Second-harmonic imaging of plant polysaccharides," J. Biomed. Opt. **10**, 024013 (2005).
6. S. W. Chu, S. Y. Chen, G. W. Chern, T. H. Tsai, Y. C. Chen, B. L. Lin and C. K. Sun, "Studies of $\chi^{(2)}/\chi^{(3)}$ tensors in submicron-scaled bio-tissues by polarization harmonics optical microscopy," Biophys. J. **86**, 3914-3922 (2004).
7. Y. Fu, H. Wang, R. Shi, and J. X. Cheng, "Second harmonic and sum frequency generation imaging of fibrous astroglial filaments in ex vivo spinal tissues," Biophys J. **92**, 3251-3259 (2007).
8. S. Psilodimitrakopoulos, S. Santos, I. Amat-Roldan, A. K. N. Thayil, D. Artigas, and P. Loza-Alvarez, "In vivo, pixel-resolution mapping of thick filaments' orientation in nonfibrilar muscle using polarization-sensitive second harmonic generation microscopy," J. Biomed. Opt. **14**, 014001 (2009).
9. D. E. Rudy, T. A. Yatskievych, P. B. Antin and C. C. Gregorio, "Assembly of thick, thin, and titin filaments in chick precardiac explants," Dev. Dyn. **221**, 61-71 (2001).

10. C. Odin, T. Guilbert, A. Alkilani, O. P. Boryskina, V. Fleury, and Y. Le Grand, "Collagen and myosin characterization by orientation field second harmonic microscopy," Opt. Express **16**, 16151-16165 (2008), http://www.opticsinfobase.org/oe/abstract.cfm?URI=oe-16-20-16151.
11. J. C. Sparrow, and F. Schock, "The initial steps of myofibril assembly: integrins pave the way," Nat. Rev. Mol. Cell Biol. **10**, 293-298 (2009).
12. R. Craig and J. L. Woodhead, "Structure and function of myosin filaments," Curr. Opin. Struct. Biol. **16**, 204-212 (2006).
13. R. Craig, and R. Padron, *Molecular structure of the sarcomere* (McGraw-Hill, New York, 2004).
14. S. G. Page, and H. E. Huxley, "Filament Lengths in Striated Muscle," J. Cell Biol. **19**, 369-390 (1963).
15. F. Vanzi, M. Capitanio, L. Sacconi, C. Stringari, R. Cicchi, M. Canepari, M. Maffei, N. Piroddi, C. Poggesi, V. Nucciotti, M. Linari, G. Piazzesi, C. Tesi, R. Antolini, V. Lombardi, R. Bottinelli, and F. S. Pavone, "New techniques in linear and non-linear laser optics in muscle research," J. Muscle Res. Cell Motil. **27**, 469-479 (2006).
16. S. V. Plotnikov, A. M. Kenny, S. J. Walsh, B. Zubrowski, C. Joseph, V. L. Scranton, G. A. Kuchel, D. Dauser, M. Xu, C. C. Pilbeam, D. J. Adams, R. P. Dougherty, P. J. Campagnola, and W. A. Mohler, "Measurement of muscle disease by quantitative second-harmonic generation imaging," J Biomed. Opt. **13**, 044018 (2008).
17. F. Légaré, C. Pfeffer, and B. R. Olsen, "The role of backscattering in SHG tissue imaging," Biophys. J. **93**, 1312-1320 (2007).
18. E. Ralston, B. Swaim, M. Czapiga, W. L. Hwu, Y. H. Chien, M. G. Pittis, B. Bembi, O. Schwartz, P. Plotz, and N. Raben, "Detection and imaging of non-contractile inclusions and sarcomeric anomalies in skeletal muscle by second harmonic generation combined with two-photon excited fluorescence," J. Struct. Biol. **162**, 500-508 (2008).
19. T. Boulesteix, E. Beaurepaire, M. P. Sauviat, and M. C. Schanne-Klein, "Second-harmonic microscopy of unstained living cardiac myocytes: measurements of sarcomere length with 20-nm accuracy," Opt. Lett. **29**, 2031-2033 (2004).
20. M. Both, M. Vogel, O. Friedrich, F. von Wegner, T. Kunsting, R. H. Fink, and D. Uttenweiler, "Second harmonic imaging of intrinsic signals in muscle fibers in situ," J. Biomed. Opt. **9**, 882-892 (2004).
21. S. V. Plotnikov, A. C. Millard, P. J. Campagnola, and W. A. Mohler, "Characterization of the myosin-based source for second-harmonic generation from muscle sarcomeres," Biophys. J. **90**, 693-703 (2006).
22. C. Greenhalgh, N. Prent, C. Green, R. Cisek, A. Major, B. Stewart, and V. Barzda, "Influence of semicrystalline order on the second-harmonic generation efficiency in the anisotropic bands of myocytes," Appl. Opt. **46**, 1852-1859 (2007).
23. N. Prent, C. Green, C. Greenhalgh, R. Cisek, A. Major, B. Stewart, and V. Barzda, "Intermyofilament dynamics of myocytes revealed by second harmonic generation microscopy," J. Biomed. Opt. **13**, 041318 (2008).
24. T. Shimizu, J. E. Dennis, T. Masaki, and D. A. Fischman, "Axial Arrangement of the Myosin Rod in Vertebrate Thick Filaments: Immunoelectron Microscopy with a Monoclonal Antibody to Light Meromyosin," J. Cell Biol. **101**, 1115-1123 (1985).
25. Max Born & Emil Wolf, *Principles of Optics: Electromagnetic Theory of Propagation, Interference and Diffraction of Light* (Pergamon Press, 6th Edition, Oxford, 1980).
26. J. W. Sanger, S. M. Kang, C. C. Siebrands, N. Freeman, A. P. Du, J. S. Wang, A. L. Stout, and J. M. Sanger, "How to build a myofibril," J. Muscle Res. Cell Motil. **26**, 343-354 (2005).
27. S. G. Mallat, *A wavelet tour of signal processing* (Academic Press, 2nd Edition, London, 1999).
28. L.D. Taylor and E. Bandman, "Distribution of fast myosin heavy chain isoforms in thick filaments of developing chicken pectoral muscle," J. Cell Biol. **108**, 533 - 542 (1989).
29. R. W. Ogilvie, R. B. Armstrong, K. E. Baird, and C. L. Bottoms, "Lesions in the rat soleus muscle following eccentrically biased exercise," Am. J. Anat. **182**, 335-346 (1988).
30. J. L. Thompson, E. M. Balog, R. H. Fitts, and D. A. Riley, "Five myofibrillar lesion types in eccentrically challenged, unloaded rat adductor longus muscle - A test model," Anat. Record **254**, 39-52 (1999).
31. I. Agarkova, E. Ehler, S. Lange, R. Schoenauer, and J. C. Perriard, "M-band: a safeguard for sarcomere stability?," J. Muscle Res. Cell Motil. **24**, 191-203 (2003).
32. S. K. Powers, A. N. Kavazis, and K. C. DeRuisseau, "Mechanisms of disuse muscle atrophy: role of oxidative stress," Am J Physiol Regul Integr Comp Physiol **228**, R337-R344 (2005).
33. A. M. Solomon and P. M. G. Bouloux, "Modifying muscle mass - the endocrine perspective," J. Endocrinol. **191**, 349-360 (2006).
34. I. Freund, M. Deutsch, and A. Sprecher, "Connective tissue polarity. Optical second-harmonic microscopy, crossed-beam summation, and small-angle scattering in rat-tail tendon," Biophys. J. **50**, 693-712 (1986).
35. W. H. Press, B. P. Flannery, S. A. Teukolsky and W. T. Veterlin, *Numerical Recipe* (Cambridge University Press, Cambridge, 1986).
36. D. Rhee, J. M. Sanger, and J. W. Sanger, "The premyofibril: evidence for its role in myofibrillogenesis," Cell Motil. Cytoskeleton **28**, 1-24 (1994).
37. J. W. Sanger, J. Wang, B. Holloway, A. Du, and J. M. Sanger, "Myofibrillogenesis in skeletal muscle cells in zebrafish," Cell Motil Cytoskeleton, Epub ahead of print (2009).

38. A. Oppenheim, R.W. Schafer, *Digital Signal Processing* (Prentice-Hall, Englewood Cliffs, 1975).

1. Introduction

Second harmonic generation (SHG) imaging microscopy has recently emerged as a powerful and unique non-destructive imaging tool for high-resolution, high-contrast, three-dimensional studies of endogenous proteins such as myosin, collagen, tubulin (microtubule), glial fibrillary acidic protein, starch, cellulose and holds promise for both basic research and clinical pathology [1–8]. SHG imaging microscopy relies on a nonlinear interaction of tightly focused ultrashort laser pulses with noncentrosymmetric quasi crystalline arrangement of optically hyperpolarizable molecules (harmonophores) causing scattered coherent radiation at twice the fundamental frequency. SHG is essentially an instantaneous phemomenon compared to fluorescence and all the incoming energy is converted into radiated photons. No nonradiative processes are involved in SHG and in consequence live cells do not suffer from phototoxic effects or photobleaching and therefore viability is extended. Moreover SHG imaging microscopy offers intrinsic optical studies of 3D endogeneous proteins which often required exogenous immunofluorescence labeling with poor optical contrast and invasiveness [9]. Finally polarization dependence of the SHG signal can be exploited as a new source of contrast to gain information from orientation and submicrometric organization of endogenous proteins [4, 10].

Striated muscles are built from very thin ($\approx 1\mu m$) contractile myofibrils formed by a regular assembly along their main axis of elementary contractile units called sarcomeres. Parallel myofibrils, separated from each other by sarcoplasmic reticulum (thickness about 200 nm), assemble laterally and are aligned at the Z-band [11] as illustrated in Fig. 1(a). They display in phase-contrast light microscopy a pattern of alternating light (I) and dark (A) bands whose striations arise as a result of the packing arrangment of the different filaments in the sarcomere [12]. Structural organization at nanometric scale of their proteins has been provided by X-ray and electron microscopy (EM) [12, 13] and it consists of a double, overlapping, hexagonal array of a large number ($\approx$ 1000) of bipolar thick (myosin) and thin (actin) filaments. Thin actin filaments are anchored at one end at Z-band while interdigitating between the thin filaments are bipolar thick filaments composed of contractile myosin also connected at the Z-band via the flexible titin protein (Fig. 1(b)). Myosin II is an hexamer (Fig. 1(c)) of two heavy chains and four light chains. The C-terminal of each heavy chain is α helical, whereas its N-terminal is globular. The two heavy chains assemble to form a coiled-coil dimer characterized by two globular heads (subfragment S1), a motor domain which hydrolyzes ATP upon contraction and binds to actin, a subfragment S2 and a tail called light meromyosin (LMM). Subfragment S2 acts as a flexible link between the head and LMM which self associates to form antiparallel tail coiled-coil interaction at the middle of the thick filament corresponding to the M-band (Fig. 1(d)). Finally thick filament elongates by staggered association of myosin tails and has a constant length of about 1.6 μm in vertebrates [14].

Coherent emission from myosin molecules of thick filaments is responsible of the characteristic periodical sarcomeric SHG signal observed in striated muscles. Surprisingly the SHG pattern is not always identical and is either one-band or two-band centered at the midlle of the sarcomere. Single-band sarcomeric SHG pattern has been observed in gastrocnemius of adult xenopus [4], frog tibialis anterior muscle [15], mouse quadriceps or gastrocnemius muscles [16, 17], mouse and human hind lamb muscles [18], veal cutlet muscles [10], nematode body-wall muscles [8]. Double-band sarcomeric SHG pattern has been observed in C-elegans body-wall muscles [1, 3], frog heart muscles [19], mouse tibialis anterior muscle [20], mouse leg and chicken heart [21], rabbit psoas muscles [15], drosophilla flight muscles [22, 23]. Such change of the sarcomeric SHG pattern is puzzling since it is well known from electron microscopy (EM) studies that the size of thick filaments is constant and that of the M-band is

between (120-200 nm) in vertebrates [12–14, 24]. In order to understand the sarcomeric SHG pattern and the conditions of its change, we undertook a quantitative study of the sarcomeric SHG signal taking into account the influence of animal species (rat versus xenopus), age (adult versus larval) and tissue preparation (fixed or fresh) using high optical resolution objectives. We found that the sarcomeric SHG signal could be either one peak or two peaks independently of the experimental conditions. Proportion of sarcomeres with one peak is the most frequent result and has been measured to be about 85%. Using α-actinin immuno detection of the Z-band, we observed that SHG intensity profiles with two peaks per sarcomere could originate from either mini sarcomeres (half of a sarcomere) or mature sarcomeres. We show that double peak SHG pattern is dramatically increase by muscle proteolysis. We discuss the biological meaning of the double peak SHG patterns.

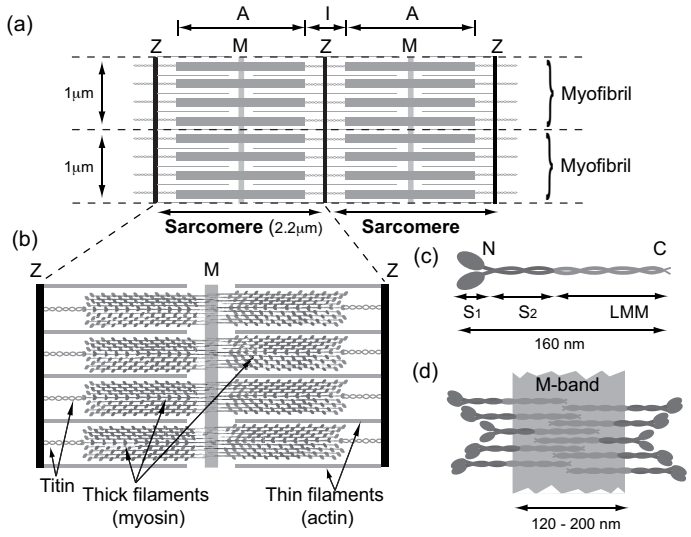

Fig. 1. Schematic diagram illustrating the major sarcomeric components of striated muscles. (a) Global view of two myofibrils (thickness $\approx 1\ \mu m$) formed by contractile sarcomeres (width $\approx 2.2\ \mu m$) which assemble laterally and display a pattern of alternating light (I) and dark (A) bands. (b) View of the sarcomere showing overlapping arrays of bipolar myosin thick filaments and actin thin filaments. Thick and thin filaments are transversally interconnected at the M- and Z- band respectively. Myomesin or M-protein (M-band) involved in these connections are not represented. Thick filaments are longitudinally connected at the Z- and M- band by titin and for simplicity only the connection at the Z-band is represented. (c) The myosin molecule is an hexamere of two heavy chains and two pairs of light chains (not presented) and has a length of about 160 nm. The heavy chain α-helix tails of each myosin molecule form a coiled-coil super helix dimer. (d) Schematic representation of the antiparallel assembly of myosin molecules at the M-band free of heads (width $\approx$ 120-200 nm). Myosin heads point away from the filament center and myosin tails have antiparallel overlapping (width 85 -130 nm).

2. Experimental methods

2.1. Tissue preparation

Muscle tissues were obtained from gastrocnemius of adult *Xenopus laevis* (national breeding facility of xenopus animals in Rennes, France) and wistar rats (Janvier, Le Genest-St-Isle-France).

At least five adult xenopus and rats were used. The tissues were fixed with paraformaldehyd (PFA) 4% (by incubation of the tissue block or by perfusion of the fixative with heparin in the whole animal prior to dissection of the muscle) or either fresh. For fixed tissues, muscles were dissected, fixed over night at 4°C then rinsed at least three times with the appropriate saline buffer (e. g. Phosphate Buffer Saline (PBS) for rat tissues and Mark's Modified Ringer (MMR) for xenopus tissues). For proteolysis analysis of muscle tissues, stage 50 tadpoles were euthanized in MS222 (0.5 mg/mL). They were either immediately fixed (J0) in PFA (4 % at 4°C) or led in breeding water at room temperature (18-22°C) for 24 H (J1) or 48 H (J2) before being fixed according to the same procedure. They were rinsed after one night of fixation in MMR saline buffer before slicing. 100 or 200 μm thick tissues were obtained by slicing muscles directly glued on the stage of a vibroslicer (LEICA, VT 1200S). Particular care has been taken to cut the slices along the main axis of the myofibrils. Slices were mounted between two coverslips in mounting medium (Vectashild, Vector Burlingame, CA) before SHG imaging. For α-actinin immunostaining, 10-15 μm cryostat sections, mounted on gelatin coated coverslips, were permeabilized with buffer containing 0.5% triton and 5% fetal calf serum for 10 minutes and incubated at 4°C over night in MMR containing 0.1% triton, 5% fetal calf serum and α-actinin antibody (1:100, mouse monoclonal IgM, ab9465, Abcam, Cambridge, MA, USA). Slices were rinsed three times in MMR and incubated at 4°C over night in Ringer containing 0.1% triton, 5% fetal calf serum and secondary antibody (1:100, Alexa Fluor 488 goat anti-mouse IgG, A11029, Molecular Probes, Eugene, OR, USA). After being rinsed three times, the tissue was covered with a drop of mounting medium (Vectashield, Vector Burlingame, CA) and a second coverslip was laid on. After being sealed, preparations were imaged.

2.2. Imaging system

Images were acquired on PIXEL (http://pixel.univ-rennes1.fr/) facility of GIS EUROPIA, University of Rennes1, France) based on either a Leica TCS SP2 confocal scanning head coupled to a DMIRB inverted microscope or an Olympus FV1000 confocal scanning head coupled to a BX61WI upright microscope. Each setup is equipped with a MAITAI Spectra Physics femtosecond laser. High numerical aperture objective either Leica 63X, oil immersion, NA 1.4, HCX PLAPO or Olympus 60X, water immersion, NA1.2, UplanApo/IR or Olympus NA1.1, LUMFl were used for applying 10-20 mW of 940 nm excitation at the sample. The theoretical optical resolution was about 400 nm, 480 nm and 520 nm for the three objectives respectively [25]. The SHG signal was collected in a forward direction using either a multi-immersion S1 (NA = 0.90-1.4) Leica condenser or an Olympus WI-UCD universal condenser (NA = 0.80). A BG39 bandpass filter and a 470 nm IR filter (10 nm FWHM) were placed before the PMT. The dichroic filter wheel of the microscope was removed and replaced by a computer control PR50CC Newport rotation stage (precision 0.1°) equiped with an achromatic zero-order Quartz-MgF_2 half-wave plate in order to adjust the polarization angle of the incident IR electric field without movement of the biological specimen. The images were quantitatively analyzed with open source ImageJ software (http://rsb.info.nih.gov/ij/). All the specimens were positionned on the fixed X,Y stage of the microscope with light propagating in the Z direction. The Olympus setup was used only for the experiments concerning the effect of proteolysis on SHG signal.

2.3. Quantification of single-band sarcomeres

To quantify the percentage of sarcomeres presenting SHG signal with one peak or two peaks per sarcomere, we have used two methods described in Appendix based respectively on a FFT analysis followed by a two-band pass Gabor filtering (Appendix 1) and an intensity profile analysis (Appendix 2). The values of Table 1 were obtained from 5 to 24 thick slices randomly

chosen from at least five animals for each experimental condition with randomized acquisition fields.

3. Experimental results

It has already been shown that the sarcomeric SHG pattern can present either one band [4, 8, 10, 16–18] or two bands [1, 3, 15, 19–23]. In order to elucidate the mechanism underlying this variation, we have extensively characterized the SHG signal from 100 μm thick slices of xenopus and rat muscles. Typical SHG images from both tissues are shown in Fig. 2(a,b). In

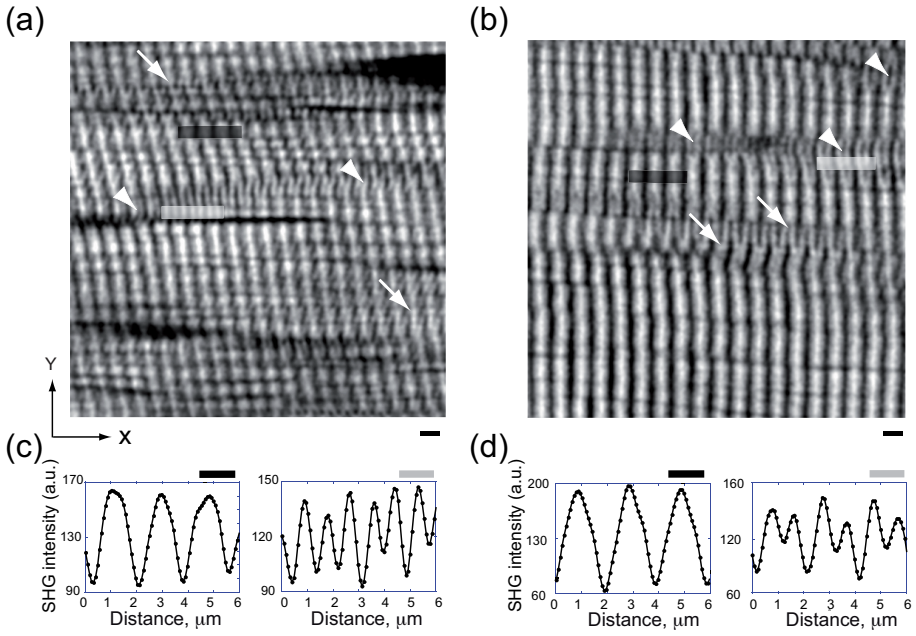

Fig. 2. Typical SHG images and intensity profiles from adult gastrocnemius muscles. (a) Optical sections illustrating SHG images from xenopus (a) and rat (b) muscles. The scale bar is 2 μm and the full image is 40×40 μm. A Gaussian Blur filter (radius=2) was applied for each image. Arrowheads and arrows indicate respectively bright double-band sarcomeric SHG signal and bright pitchfork SHG pattern. (c, d) SHG intensity profiles along the indicated segments in respectively (a) and (b). The left and right profiles of images (c) and (d) correspond respectively to the horizontal black and white lines drawn in (a) and (b). Note that the optical resolution was not sufficient to discriminate indiviual myofibrils that are horizontally aligned.

most regions, sarcomeric SHG signals are bright straight bands regularly spaced orthogonally to the long axis of each myofibril oriented along the horizontal X axis of the microscope stage. One can also noticed in some regions the presence of a regular pattern with the same spacing but presenting two bands (see arrowheads). Corresponding SHG intensity profiles presented in Fig. 2(c,d) along indicated segments of Fig. 2(a,b) clearly show that within the same spacing ($\approx 2\ \mu m$) the SHG pattern present either one peak or two peaks. We undertook immuno staining of α-actinin which is considered as a specific molecular marker of Z-band [21, 26]. TPEF signal was found to periodically alternate with sarcomeric SHG signal as illustrated in Fig. 3 demonstrating that SHG signal can effectively be either one band or two bands per sarcomere. Two methods were used to quantify the proportion of each pattern. The first one (see Appendix

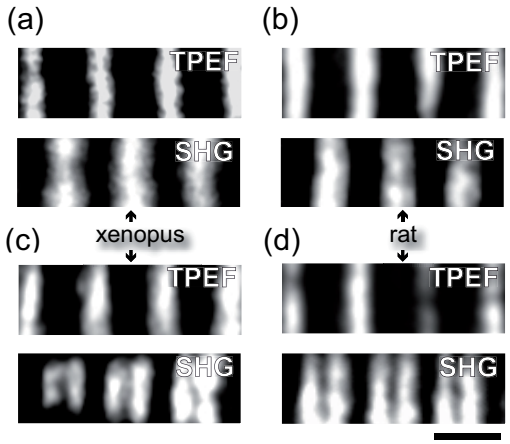

Fig. 3. Typical sarcomeric TPEF and SHG signal of gastrocnemius muscles. Single-band (a,b) and double-band (c,d) sarcomeres from xenopus (a,c) and rat (b,d). The upper and lower panels of (a-d) correspond respectively to α-actinin TPEF and myosin SHG signals. Scale bar (2 μm).

1) is based on a FFT analysis followed by a local two band-pass Gabor filtering [27] which enhances the spectral components associated to sarcomeres with one band or two bands. A post-filtering decision stage enables to automatically classify each pixel in one of three classes: background, single-band sarcomere and double-band sarcomere. The second one (see Appendix 2) is based on the detection of the maximum of the SHG intensity profile corresponding to a transition between a positive and a negative first discrete derivative. This later method classify SHG pattern in two categories: pattern with one band per sarcomere or pattern with two bands per sarcomere. The results, given in Table 1 for the analyzed samples, show that single-band sarcomeric SHG pattern is the predominant feature (85%) of most sarcomeres for adult rat and xenopus. For xenopus, this result is independent of the method of tissue preparation and is identical for two weeks old tadpole fresh tail muscles. Note that the two independently designed methods yield the same result demonstrating their efficiency.

It has been shown [4, 8, 10, 21] that in muscles SHG signal originates from the single α-helix of myosin thick filaments and in consequence the SHG signal is supposed to extend along the A-band except at the M-band where myosin tail-tail interaction occurs (see Fig. 1(d)). Indeed destructive interferences are created in this region which could reduce the SHG signal at the center of the sarcomere as it has been reported [1, 19, 21]. The size of the M-band was found to vary between 120 nm and 200 nm in vertebrates and it is important to note that the antiparallel packing region of myosin tail molecules is always lower and has been estimated to be between 85 - 130 nm [12, 24]. Both the size of the antiparallel packing and the value of the optical resolution which is far greater ($\approx$ 400 nm) explain 1/ no visible attenuation of the SHG signal due to centrosymmetry was detected at the center of the sarcomere and 2/ predominance of single-band sarcomeric SHG pattern. The second feature of the results (see Table 1) is that about 15% of the sarcomeric SHG patterns present two bands as already observed in previous studies. As it was already mentioned, the optical resolution is not sufficient to observe a significant dip due to intra A-band centrosymmetry. This conclusion is also supported by the lack of optical resolution to distinguish each myofibril wrapped by $\approx$ 200 nm thick sarcoplasmic reticulum [14]. On the other hand we have measured the distance between the two peaks within each sarcomere and we found that this distance varies from 0.6 μm to 1.2 μm in agreement

Table 1. Quantification of sarcomeric SHG patterns in xenopus and rat muscles. The first two lines represent the mean percentage and standard deviation ($\pm$ SD) of single-band (SB) sarcomeres from xenopus gastrocnemius (X Gastroc), xenopus tail (X tail) and rat gastrocnemius (R Gastroc) muscles. The tissues were fixed with PFA 4% (incubated or perfused) or either fresh. Note that the mean percentage has been determined using the Gabor filtering method (Gabor) or the intensity profile analysis (IPA) presented in Appendix 1 and Appendix 2 respectively. The values were obtained from 5 to 24 thick slices ($40\times40\times10$ μm^3) from at least five animals for each experimental condition. The mean sarcomere size ($\pm$ SD) and the average ($\pm$ SD) full width at half maximum (FWHM) of the sarcomeric SHG signal were determined for both single-band (SB) and double-band (DB) sarcomeres for each experimental condition.

	X Gastroc incubated	X Gastroc perfused	X tail Fresh	R Gastroc incubated
Mean percentage of SB sarcomeres (%) - Gabor	75$\pm$21	91$\pm$10	96$\pm$3	84$\pm$7
Mean percentage of SB sarcomeres (%) - IPA	81$\pm$17	83$\pm$5	95$\pm$6	84$\pm$8
Size of SB sarcomeres (μm)	1.9$\pm$0.1	2.2$\pm$0.1	2.4$\pm$0.2	2.1$\pm$0.1
Size of DB sarcomeres (μm)	1.9$\pm$0.1	2.2$\pm$0.1	2.5$\pm$0.2	2.0$\pm$0.1
FWHM of the SHG signal for SB sarcomeres (μm)	1.1$\pm$0.1	1.1$\pm$0.2	1.3$\pm$0.1	1.2$\pm$0.1
FWHM of the SHG signal for DB sarcomeres (μm)	1.4$\pm$0.1	1.5$\pm$0.1	1.6$\pm$0.1	1.4$\pm$0.1

with estimated results from previous studies [1, 3, 15, 19–23]. It seems unlikely that such large amplitude separation could be due to intra A-band centrosymmetry and the double peak SHG pattern that we observed should have an other explanation. It has also been suggested, in body wall muscles of C. elegans, that a non uniform distribution of myosin heavy chain isoforms along each thick filament could explain the central dip of the sarcomeric SHG signal since the isoform with the lowest SHG efficiency is localized at the center of the A-band [1, 3]. Non uniform distribution of myosin heavy chain isoforms has also been shown in chicken pectoralis thick filaments [28]. However in vertebrates (including xenopus and rats) the effect of such asymmetric distribution on the sarcomeric SHG intensity still needs to be studied. Alternative explanations of the dip are also possible and will be discussed below. Whereas the mean size of the sarcomeres were identical, we observed that the full width at half maximum (FWHM) of the sarcomeric SHG intensity profile was significantly higher ($\approx$ 25%) for double-band versus single-band sarcomeres in each experimental condition (see Table 1). This result indicates that the signal originates from an extended region within the sarcomere. In normal physiological condition the thick filaments within the sarcomere ($\approx$1000) are all aligned by titin and M-band proteins. In extra physiological eccentric contraction, misalignment of A-band thick filaments has been observed at EM level [14, 29, 30]. The increase of the width of the SHG signal and the presence within the sarcomere of two well separated SHG peaks could originate from A-band thick filaments disorder. Indeed it has been proposed that double-band sarcomeric SHG signal could be due to thick filament proteolysis and disassembly in human patient with pompe disease [18]. To evaluate this hypothesis, we have studied the effect of proteolysis on sarcomeric SHG signal from xenopus tadpole tail muscles. As illustrated in Fig. 4, we found a significant increase (about five fold) of the proportion of double-band sarcomeric SHG signal (see Table 2) after one day of tissue degradation (see Experimental methods). The FWHM for double-band sarcomeres were about 30% higher than that of single-band sarcomeres in agreement with the results of Table 1. Almost all sarcomeres were converted to double-band SHG sarcomeres after two days of degradation. It is well known that over exercice, eccentric contraction, muscle disease, stress and reactive oxygen species production induce proteolysis and thick filaments disassembly [31, 32]. Titin and M-band proteins are elastic molecules that respectively center

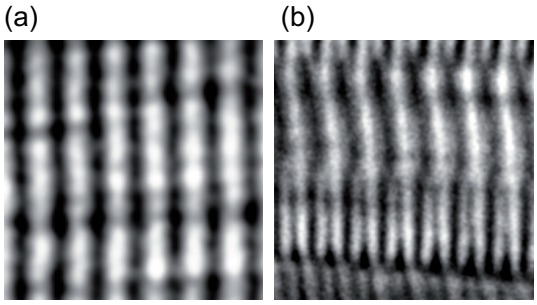

Fig. 4. SHG images illustrating the effect of 1 day proteolysis on sarcomeric SHG patterns of xenopus tail muscles. (a) Control without proteolysis (J0). (b) After 24H proteolysis (J1). Each image is 13×13 μm.

and align myosin thick filaments and at the begining of pretolysis these proteins are the first to be broken inducing disassembly and misalignment of A-band thick filaments [30–32]. At this first stage of pretolysis, thick filaments which are not degraded could be disorganized generating a supra A-band thick filament centrosymmetry in the central region of the sarcomere. Destructive interferences could originate from this disorganization resulting in the apparition of a central dip in the sarcomeric SHG pattern. In normal condition adult muscle tissue undergoes regeneration and degeneration with assembly and disassembly of sarcomeres [33]. A significant fraction of the double-band SHG patterns observed on xenopus and rat muscles in normal physiological condition could be related to these regeneration and degeneration processes.

Table 2. Quantification of the effect of proteolysis on sarcomeric SHG patterns in xenopus tail muscles. The values represent the mean percentage and standard deviation ($\pm$ SD) of single-band (SB) sarcomeres from xenopus tail (X tail) muscles. J0 is the control without proteolysis, J1 and J2 correspond respectively to 24 H and 48H proteolysis. The values were obtained from 5 to 12 thick slices from two or three animals for each experimental condition.

	X tail J0 incubated	X tail J1 incubated	X tail J2 incubated
Mean percentage of SB sarcomeres (%) - Gabor	94$\pm$8	59$\pm$12	13$\pm$8
Mean percentage of SB sarcomeres (%) - IPA	93$\pm$11	66$\pm$17	6$\pm$7

A close look of Fig. 2(a-b) indicates that two distinct double-band SHG patterns can be observed. The first one is a genuine double-band sarcomeric SHG pattern (see arrowheads in Fig. 2(a,b)) as illustrated in Fig. 3(a-d) and the second one is a pitchfork-like pattern (see arrows in Fig. 2(a,b)). The quantification method did not discriminate between these two patterns because of their same spatial frequency and it should be noted that these patterns represent the 15% value of double-band sarcomeres given in Table 1. We have discussed above the possible mechanisms leading to a double-band sarcomeric SHG pattern and one can wonder if the pitchfork-like pattern could be also generated by the same mechanisms? In order to characterize this pattern, we undertook immuno staining of α-actinin (marker of the Z-band). The corresponding TPEF signal was found to periodically alternate with SHG signal as illustrated in Fig. 5 with 50% reduction of both the distance between two adjacent Z-bands (see arrows) and of the width of the SHG signal of the corresponding A-bands (see arrowheads) revealing

the presence of mini sarcomeres. We were unable with α-actinin immuno staining to mark all

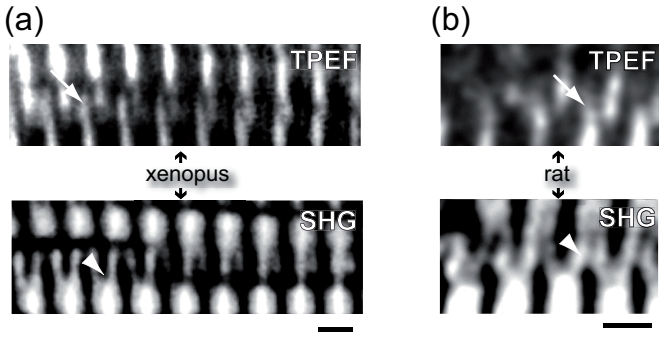

Fig. 5. TPEF α-actinin analysis of regions with pitchfork-like SHG pattern of gastrocnemius muscles and diagram of myofibrils with mature and mini sarcomeres. Upper (TPEF) and lower (SHG) panels are respectively from xenopus (a) and rat (b). Note the progressive alignment of the Z-band from left to right in (a) suggesting maturation of the myofibril. Scale bar (2μm).

the Z-bands of the thick tisues due to antigene accessibility and photo-bleaching. Nethertheless each time TPEF immuno staining revealed mini sarcomeres they were found in regions of pitchfork-like SHG pattern. It is therefore reasonnable to associate pitchfork-like SHG pattern with mini sarcomeres. On can also notice that in regions of pitchfork-like pattern, we observed misalignment and disconnection of α-actinin fluorescence staining and continuity of the myosin SHG signal between adjacent myofibrils with a visible angle ($\approx 30^\circ$) (see arrowheads in Fig. 5). This angle suggests that the orientation of thick filaments between mini and mature sarcomeres could be different. To probe this orientation, we undertook a polarization dependence study of the SHG signal in a region containing pitchfork-like structures (see Fig. 6(a)). Indeed polarization dependence of the SHG signal is a very sensitive probe of the orientation of harmonophores [4, 6, 34] and would detect any change in the orientation of myosin molecules. As expected, the SHG intensity varies (see Fig. 6(b)) with the orientation of the incident IR electric field identically inside and outside the pitchfork-like structure suggesting identical orientation of A-band thick filaments between adjacent myofibrils. The SHG intensity in three selected ROIs ▲, ● and ■ localized respectively in the lower, upper and median arms of the pitchfork-like structure of Fig. 6(a) was plotted in Fig. 6(c) as a function of the polarization angle of the incident IR electric field. The result shows that the variation of the SHG intensity is identical for all ROI's. We have adjusted the experimental data with the following theoretical model [4] describing the evolution of the SHG intensity $I^{2\omega}$ for polar filaments

$$I^{2\omega} \sim [\sin^2 2\alpha + (\sin^2\alpha + \frac{\chi_{33}}{\chi_{15}}\cos^2\alpha)^2]. \quad (1)$$

In this equation, α is the angle between the incident IR electric field and the main axis of the myofibrils which corresponds to the X axis of the laboratory coordinates (X, Y, Z) (see the inset of Fig. 6(c)). This alignement was performed outside the regions of pitchfork-like pattern. In the above equation χ_{33}, χ_{31}=χ_{15} are the two independent macroscopic nonlinear susceptibility coefficients assuming a dominant axial hyperpolarizability coefficient and a cylindrical symmetry of myosin molecules along the main axis X of the myofibrils. We have used a nonlinear least-squares fit with the Levenberg-Marquardt method [35] in order to adjust the fitting parameter χ_{33}/χ_{15} with the experimental data of Fig. 6(c). We found that the fitting parame-

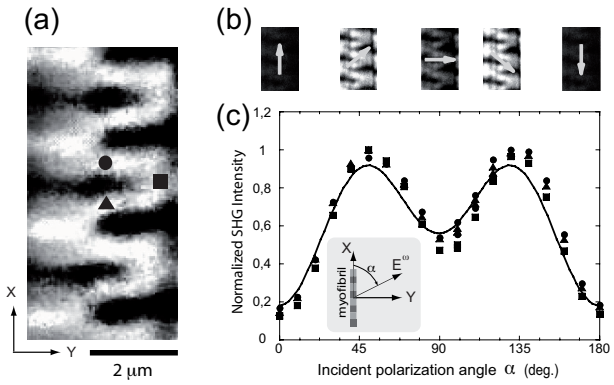

Fig. 6. Polarization dependence study of the SHG signal in regions with pitchfork-like structures. (a) Typical SHG pitchfork-like pattern. (b) SHG optical sections illustrating the effect of five different incident polarization angles α (0°, 50°, 90°, 130°, 180°) on the emitted signal from the same field of view. The arrows indicate the polarization of the incident electric field for each panel (the upperward vertical arrow represents 0°). (c) Normalized SHG signal as a function of the incident polarization angle α for ROIs ■, ▲ and ● indicated in (a). Note the correspondance between the ROIs in (a) and legend symbols in (c). The long axis of myosin filaments was oriented along the X axis of the laboratory coordinates (X, Y, Z) as shown in the inset .

ter χ_{33}/χ_{15}=0.56 was identical for all ROIs and in good agreement from the values found for myosin [4]. From this result, we conclude that the orientation of the A-band thick filaments is identical in all branches of the pitchfork which is in good agrement with the presence of mini sarcomeres revealed by immuno staining.

What could be the physiological revelance of these mini sarcomeres? The mechanism of sarcomeric proteins assembly into myofibrils is currently a matter of debate but one of the three proposed models developed by Sanger et al. [26] suggests that the size of sarcomeres changes during myofibrillogenesis and could proceed as a transition through three categories of fibrils: premyofibrils, nascent myofibrils and mature myofibrils [36, 37]. These authors suggest that premyofibrils and nascent myofibrils are mini sarcomeres. Based on the preferential localization of mini-sarcomeres in regions of pitchfork-like SHG pattern, we propose that these latter could correspond to regions of myofibrillogenesis.

4. Conclusion

In this report we have shown that the main feature of the sarcomeric SHG signal is a single peak per sarcomere (about 85% of all sarcomeres). α-actinin immuno detection of the Z-band has revealed that the remaining (15%) was either double peak per mature sarcomere or mini sarcomeres (half of a sarcomere). Mini sarcomeres are found in region of pitchfork-like SHG pattern suggesting that this pattern could be a signature of myofibrillogenesis. We show that double peak sarcomeric SHG pattern found in normal physiological conditions is enhanced during proteolysis suggesting that this pattern could be a signature of muscle degradation.

Acknowledgments

We thanks Région Bretagne, Rennes Métropole, Conseil Général d'Ille-et-Vilaine Ministére de l'enseignement supérieur et de la recherche for their financial support, Fabrice Sen-

ger, Hélène Mereau for their technical help and Emmanuel Schaub for helpful discussions.

5. Appendix 1

Gabor filtering method. In order to detect single- and double- band sarcomeres, a local spatial frequency analysis is used and manually applied to a stack. It is based on two band-pass Gabor filtering [27] which enhance the spectral components associated to single-band (frequency f_1) and double-band sarcomeres (frequency f_2). A post-filtering decision stage enables to automatically classify each pixel in one of three classes: background, single-band sarcomere and double-band sarcomere. The overall process is detailed in the following considering as an example the SHG image of Fig. 7(a).

Single- and double- band frequencies estimation. The intensity profile $I_i(x)$ is performed for each line i and the result is presented in Fig. 7(b) for lines i=208 and i=448. The single-band frequency f_1 is then estimated based on the Fast Fourier Transform (FFT) [38] of each SHG intensity profile (See Fig. 7(c)) and is deduced from the average of all FFT's of all lines (See Fig. 7(d)). The double band frequency f_2 is defined as $f_2 = 2f_1$. For example, for the SHG image of Fig. 7(a), we found f_1 = 0.55 μm^{-1}. Note that axis x is defined as the direction of the main filament axis.

Gabor filters description. Two band-pass Gabor filters $g_{f_1}(x)$ and $g_{f_2}(x)$ [27], centered on frequencies f_1 and f_2 are used (Fig. 8(a,b)) to detect significant energies around each frequency at a current position on line i of the SHG image. The filter is defined by a complex impulse response function $g_f(x) = g^r(x,f) + ig^i(x,f) = W(x)(\cos(2\pi fx) + i\sin(2\pi fx))$ equal to a complex harmonic signal at spatial frequency f ($f = f_1$ or $f = f_2$) multiplied by a Gaussian-shaped envelope $W(x) = \frac{1}{\sigma\sqrt{2\pi}}\exp(-\frac{x}{2\sigma^2})$. The dispersion parameter σ determines the Gabor filter spatial resolution around the origin and its inverse σ^{-1} determines frequency dispersion around central frequency f. The SHG image is filtered line by line by $g_{f_1}(x)$ and $g_{f_2}(x)$. The responses of these two filters to the intensity profile $I_i(x)$ of each line i provide local information on spectral components energies around f_1 and f_2 and hence on the possible presence of single- or double- band sarcomeres (See Fig. 8(c,d)). Therefore, filtering each line of the SHG image by the Gabor filters result in two filtered images (not presented) I^{f_1} and I^{f_2} highlighting single- and double- band location in this image. The gray value level of each pixel (i,j) of these filtered images are defined by $I^f(i,j) = |I_i * g_f(j)|$ for $f = f_1$ and $f = f_2$. In order to enhance signal to noise ratio I^{f_1} and I^{f_2} are smoothed with a 2D spatial rectangular mask 24×7 pixels leading to two smoothed images $I_S^{f_1}$ and $I_S^{f_2}$ presented in Fig. 8(e,f).

Decision. The goal of the decision stage is to decide for each pixel (i,j) (depending on the two values $I_S^{f_1}(i,j)$ and $I_S^{f_2}(i,j)$) if it belongs to a single-band sarcomere, a double-band sarcomere or to background. The following decision rule is used:

- if $I_S^{f_1}(i,j) + I_S^{f_2}(i,j) < T_1$: no sarcomere (the responses to the two Gabor filters are low);
- if $I_S^{f_1}(i,j) + I_S^{f_2}(i,j) \geqslant T_1$ and $I_S^{f_1}(i,j)/I_S^{f_2}(i,j) \geqslant T_2$: single-band sarcomere;
- otherwise: double-band sarcomere.

Thresholds T_1 and T_2 are typically 10 and 2. The value of T_1 is determined empirically based on the rejection of the background. $T_2 > 1$ enables to consider the fact that profiles

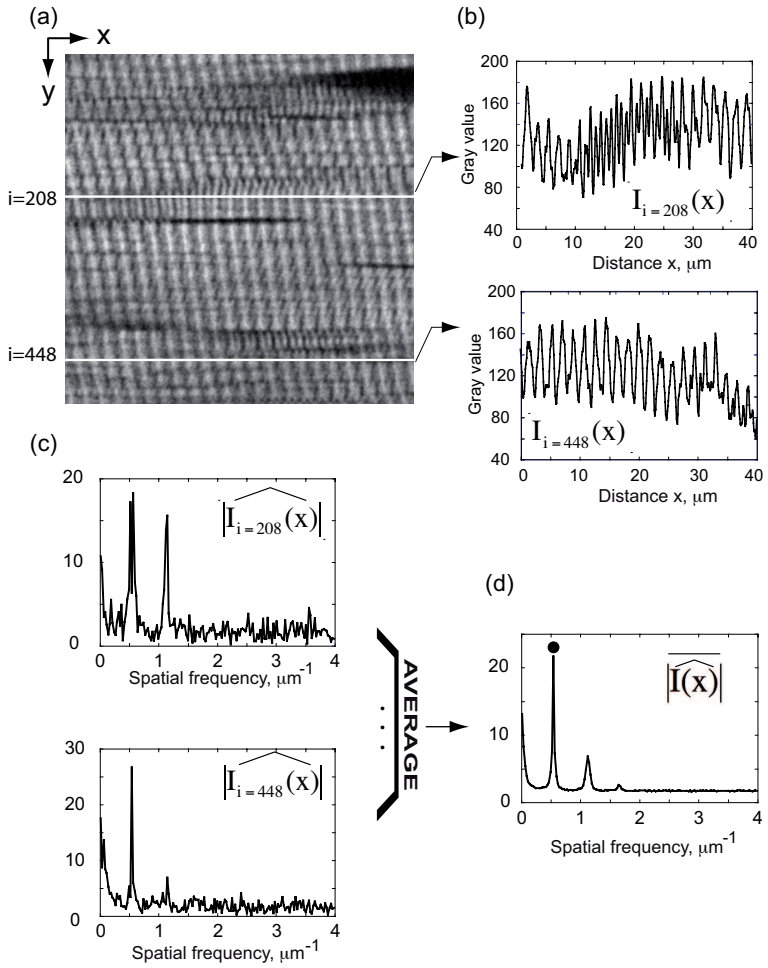

Fig. 7. Single-band and double-band frequency estimation by FFT analysis. (a) Before processing FFT's the SHG image (512×512), corresponding to that of Fig. 2(a) after a Gaussian Blur filter (radius=1), is manually rotated in order to orientate horizontally the main direction of myofibrils. The full image is 40×40 μm. (b) SHG intensity profile $I_i(x)$ for lines i=208 and i=248. (c) The modulus of the FFT, $|\widehat{I_i(x)}|$ is given for lines i=208 and i=248. Line $i = 208$ contains single- and double- band sarcomeres while line $i = 448$ contains only single-band sarcomeres. (d) In order to highlight main frequencies components, $|\widehat{I_i(x)}|$ are then averaged on all lines i providing $\overline{|\widehat{I(x)}|}$. Estimation of the single band frequency f_1 is done by the selection on $\overline{|\widehat{I(x)}|}$ of the peak corresponding to the fundamental frequency (bold circle on (d)).

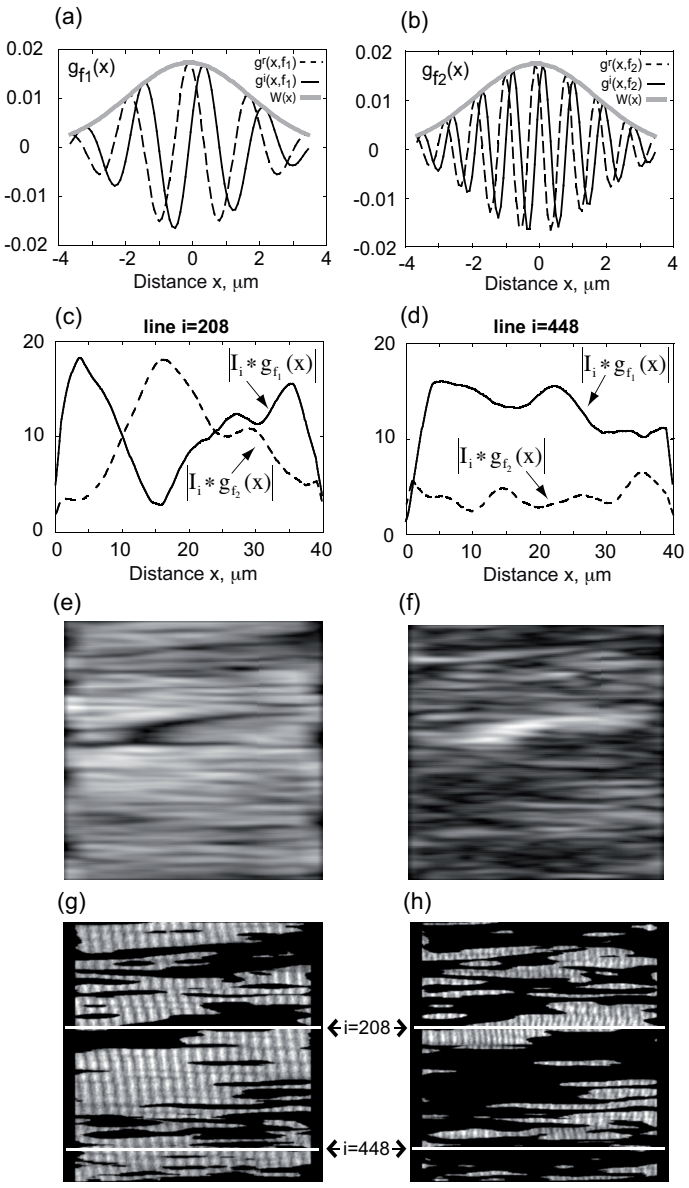

Fig. 8. Gabor filter analysis. Impulse responses of Gabor filters associated to (a) single band frequency $g_{f_1}(x) = g^r(x, f_1) + ig^i(x, f_1)$ and (b) double band frequency $g_{f_2}(x) = g^r(x, f_2) + ig^i(x, f_2)$. A high value of σ provides a precise spectral analysis but a poor spatial resolution. A good compromise is a value of σ of $\frac{1}{f_1} \approx 24$ pixels. Response of the two Gabor filters $g_{f_1}(x)$ and $g_{f_2}(x)$ for intensity profiles $I_i(x)$ of lines i=208 (c) and i=448 (d) of Fig. 7(b). Operator $*$ represents the convolution of the intensity profile with the impulse response of the Gabor filter. Single- and double- band frequency filtering f_1 and f_2 are respectively in full and dash line. Line i=208 contains single- and double- band sarcomeres while line $i = 448$ contains only single band sarcomeres. (e) and (f) represent the result of the smoothing after Gabor filtering at frequencies f_1 and f_2 applied to the SHG image of Fig. 7(a). (g) and (h) represent the result of the decision step for respectively single-band and double-band sarcomeres. Lines i=208 and i=448 considered in (c,d) are drawn in white in (g,h). In order to limit side effects caused by Gabor filtering, two vertical bands of width 24 pixels ($\frac{1}{f_1} \approx 24$ pixels) are not considered for decision in (g) and (h).

corresponding to double-band sarcomeres (frequency f_2) contain also patterns with single-band sarcomere (frequency f_1). The percentage of single-band sarcomeres of Table 1 is given by the ratio of the number of pixels belonging to single-band sarcomeres over the number of pixels belonging to single- or double- band sarcomeres. From the decision step two masks are made in order to separate pattern with single- or double- band sarcomeres in the SHG image. The result of the two masks on Fig. 7(a) is presented in Fig. 8(g,h)

6. Appendix 2

Intensity profile analysis. An algorithm was built, and a corresponding ImageJ macro was designed, to automatically compute in a stack the percentage of myofibrils with one peak per sarcomere. Care was taken to orientate horizontally the main direction of the myofibrils parallel to the X axis (See Fig. 9). Firstly a gaussian filter (radius=4) was applied to each slice *k* of the

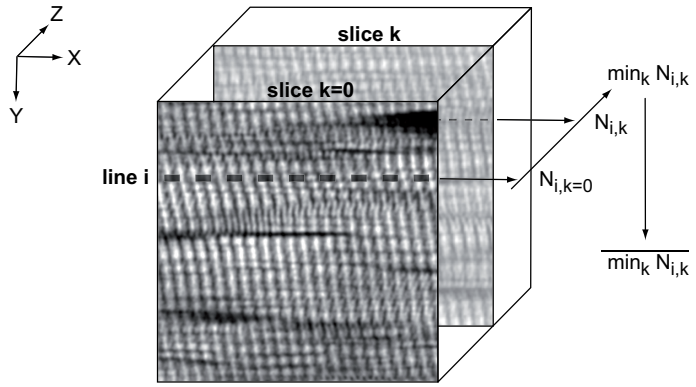

Fig. 9. Description of the method of intensity profile analysis. 3D schematic view of an entire stack where the first image of the stack corresponds to that of Fig. 2(a). Each image is oriented wih the myofibril main axis oriented along the X axis of the laboratory. The number of peaks $N_{i,k}$ of the pixel intensity profile is determined for line i of slice k. The minimum value $min_k\ N_{i,k}$ is determined for line i from all slices k and the average $\overline{min_k\ N_{i,k}}$ is deduced from all lines i.

stack. The number of peaks $N_{i,k}$ of the pixel intensity profile is computed for line i of slice k. Adjacent lines i were separated by a distance of 1 to 2 μm in order to analyze only different myofibrils (the typical myofibril diameter is about 1 μm). Identification of a peak is based on the detection of points corresponding to a transition between a positive and a negative first discrete derivative. The minimum value $min_k\ N_{i,k}$ is determined for line i from all slices k of the entire stack. The average $\overline{min_k\ N_{i,k}}$ is computed from all values of $min_k\ N_{i,k}$ of all lines i and considered as the reference number for myofibrils with one peak per sarcomere. A decision threshold (t) is taken in order to classify each myofibril as myofibril with one peak or two peaks per sarcomere using the following rule: myofibril of line *i* of slice *k* corresponds to myofibril with one peak per sarcomere if $N_{i,k} \leq (1+t) \times \overline{min_k\ N_{i,k}}$ (typically $t = 0.2$). The percentage of myofibrils with one peak per sarcomere which is reported in Table 1 is estimated for the whole stack as follow

$$\frac{card(\{(i,k) : N_{i,k} \leq (1+t) \times \overline{min_k\ N_{i,k}}\ \})}{card(\{(i,k)\})} \times 100,$$

where $card(E)$ denotes number of elements in E.